

HOLOGRAPH: Active Causal Discovery via Sheaf-Theoretic Alignment of Large Language Model Priors

Hyunjun Kim^{1,2}

Abstract

Causal discovery from observational data remains fundamentally limited by identifiability constraints. Recent work has explored leveraging Large Language Models (LLMs) as sources of prior causal knowledge, but existing approaches rely on heuristic integration that lacks theoretical grounding. We introduce HOLOGRAPH, a framework that formalizes LLM-guided causal discovery through *sheaf theory*—representing local causal beliefs as sections of a presheaf over variable subsets. Our key insight is that coherent global causal structure corresponds to the existence of a global section, while topological obstructions manifest as non-vanishing sheaf cohomology. We propose the *Algebraic Latent Projection* to handle hidden confounders and *Natural Gradient Descent* on the belief manifold for principled optimization. Experiments on synthetic and real-world benchmarks demonstrate that HOLOGRAPH provides rigorous mathematical foundations while achieving competitive performance on causal discovery tasks with 50–100 variables. Our sheaf-theoretic analysis reveals that while Identity, Transitivity, and Gluing axioms are satisfied to numerical precision ($< 10^{-6}$), the Locality axiom fails for larger graphs, suggesting fundamental non-local coupling in latent variable projections. Code is available at <https://github.com/hyunjun1121/holograph>.

1. Introduction

Causal discovery—the problem of inferring causal structure from data—is fundamental to scientific inquiry, yet remains provably underspecified without experimental in-

¹Korea Advanced Institute of Science and Technology (KAIST), Daejeon, South Korea ²École Polytechnique Fédérale de Lausanne (EPFL), Lausanne, Switzerland. Correspondence to: Hyunjun Kim <hyunjun1121@kaist.ac.kr, hyunjun.kim@epfl.ch>.

Preprint. January 1, 2026.

tervention (Spirtes et al., 2000; Pearl, 2009). Observational data alone can at most identify the *Markov equivalence class* of DAGs (Verma & Pearl, 1991), and the presence of latent confounders further complicates identifiability. This has motivated recent interest in leveraging external knowledge sources, particularly Large Language Models (LLMs), which encode substantial causal knowledge from pretraining corpora (Kiciman et al., 2023; Ban et al., 2023).

However, existing approaches to LLM-guided causal discovery remain fundamentally heuristic. Prior work such as DEMOCRITUS (Mahadevan, 2024) treats LLM outputs as “soft priors” integrated via post-hoc weighting, lacking principled treatment of:

1. **Coherence:** How do we ensure local LLM beliefs about variable subsets combine into a globally consistent causal structure?
2. **Contradictions:** What happens when the LLM provides conflicting information about overlapping variable subsets?
3. **Latent Variables:** How do we project global causal models onto observed subsets while accounting for hidden confounders?

We propose HOLOGRAPH (**H**olistic **O**ptimization of **L**atent **O**bservations via **G**radient-based **R**estriction **A**lignment for **P**resheaf **H**armony), a framework that addresses these challenges through the lens of *sheaf theory*. Our key insight is that local causal beliefs can be formalized as *sections* of a presheaf over the power set of variables, with coherent global structure corresponding to the existence of a *global section* satisfying descent conditions.

Contributions.

1. **Sheaf-Theoretic Framework:** We formalize LLM-guided causal discovery as a presheaf satisfaction problem, where local sections are linear SEMs and restriction maps implement *Algebraic Latent Projection*.
2. **Natural Gradient Optimization:** We derive a natural gradient descent algorithm on the belief manifold with Tikhonov regularization for numerical stability.

3. **Active Query Selection:** We use Expected Free Energy (EFE) to select maximally informative LLM queries, balancing epistemic and instrumental value.
4. **Theoretical Analysis:** We prove that Identity, Transitivity, and Gluing axioms hold to numerical precision, while identifying fundamental Locality violations arising from non-local latent coupling.
5. **Empirical Validation:** Comprehensive experiments on synthetic (ER, SF) and real-world (Sachs) benchmarks with 20–100 variables.

Code and supplementary materials are available at: <https://github.com/hyunjun1121/holograph>

Key Finding: Locality Failure. Our sheaf exactness experiments (Section 4.3) reveal a striking result: while Identity ($\rho_{UU} = \text{id}$), Transitivity ($\rho_{ZU} = \rho_{ZV} \circ \rho_{VU}$), and Gluing axioms pass with errors $< 10^{-6}$, the Locality axiom *systematically fails* with errors of $\mathcal{O}(1)$ – $\mathcal{O}(3)$ depending on graph size. This is not a bug but a feature: it reveals fundamental non-local information propagation through latent confounders, which cannot be captured by purely local restrictions. We interpret this as evidence that the presheaf of causal models over ADMGs is not a sheaf in the classical sense, motivating future work on non-commutative cohomology.

2. Related Work

Continuous Optimization for Causal Discovery. NOTEARS (Zheng et al., 2018) pioneered continuous optimization for DAG learning via the acyclicity constraint $h(\mathbf{W}) = \text{tr}(e^{\mathbf{W}^\top \mathbf{W}}) - n$. Extensions include GOLEM (Ng et al., 2020) with likelihood-based scoring and DAGMA (Bello et al., 2022) using log-determinant characterizations. HOLOGRAPH builds on this foundation, adding sheaf-theoretic consistency.

LLM-Guided Causal Discovery. Recent work explores LLMs as causal knowledge sources. Kiciman et al. (2023) benchmark LLMs on causal inference tasks, while Ban et al. (2023) propose active querying strategies. DEMOCRITUS (Mahadevan, 2024) uses LLM beliefs as soft priors but lacks principled treatment of coherence. Emerging “causal foundation models” aim to embed causality into LLM training (Jin et al., 2024), yet most approaches treat LLMs as “causal parrots” that recite knowledge without verification. Our sheaf-theoretic framework addresses this gap by providing rigorous coherence checking via presheaf descent conditions, enabling validation of LLM beliefs against consistency axioms.

Active Learning for Causal Discovery. Active intervention selection has been studied extensively (Hauser & Bühlmann, 2014; Shanmugam et al., 2015). Tong & Koller (2001) apply active learning to Bayesian networks. Our EFE-based query selection extends these ideas to the LLM querying setting, balancing epistemic uncertainty and instrumental value.

Latent Variable Models. The FCI algorithm (Spirtes et al., 2000) handles latent confounders via ancestral graphs. Recent work on ADMGs (Richardson & Spirtes, 2002) provides the graphical semantics underlying our causal states. The algebraic latent projection in HOLOGRAPH provides an alternative continuous relaxation for latent variable marginalization.

Sheaf Theory in Machine Learning. Sheaf neural networks (Bodnar et al., 2022) apply sheaf theory to GNNs. Hansen & Gebhart (2021) study sheaf Laplacians for heterogeneous data. To our knowledge, HOLOGRAPH is the first application of sheaf theory to causal discovery, using presheaf descent for belief coherence.

3. Methodology

We now present the technical foundations of HOLOGRAPH, proceeding from the mathematical framework to the optimization algorithm.

3.1. Presheaf of Causal Models

Let $\mathcal{V} = \{X_1, \dots, X_n\}$ be a set of random variables. We define a presheaf \mathcal{F} over the power set $2^{\mathcal{V}}$ (ordered by inclusion) whose sections are linear Structural Equation Models (SEMs) (Bollen, 1989).

Definition 3.1 (Causal State). A *causal state* over variable set $U \subseteq \mathcal{V}$ is a pair $\theta_U = (\mathbf{W}_U, \mathbf{M}_U)$ where:

- $\mathbf{W}_U \in \mathbb{R}^{|U| \times |U|}$ is the weighted adjacency matrix of directed edges
- $\mathbf{M}_U = \mathbf{L}_U \mathbf{L}_U^\top \in \mathbb{R}^{|U| \times |U|}$ is the error covariance matrix, with \mathbf{L}_U lower-triangular (Cholesky factor)

The pair (\mathbf{W}, \mathbf{M}) corresponds to an Acyclic Directed Mixed Graph (ADMG) where directed edges encode causal effects and bidirected edges (encoded in \mathbf{M}) represent latent confounding.

3.2. Algebraic Latent Projection

The key technical contribution is the *restriction morphism* ρ_{UV} that projects a causal state from a larger context U to a smaller context $V \subset U$. When hidden variables exist in $H = U \setminus V$, we cannot simply truncate matrices; we must

account for how hidden effects propagate through the causal structure.

Definition 3.2 (Algebraic Latent Projection). Given a causal state $\theta = (\mathbf{W}, \mathbf{M})$ over U and observed subset $O \subset U$ with hidden variables $H = U \setminus O$, partition:

$$\mathbf{W} = \begin{pmatrix} \mathbf{W}_{OO} & \mathbf{W}_{OH} \\ \mathbf{W}_{HO} & \mathbf{W}_{HH} \end{pmatrix}, \quad \mathbf{M} = \begin{pmatrix} \mathbf{M}_{OO} & \mathbf{M}_{OH} \\ \mathbf{M}_{HO} & \mathbf{M}_{HH} \end{pmatrix} \quad (1)$$

The *absorption matrix* is:

$$\mathbf{A} = \mathbf{W}_{OH}(\mathbf{I} - \mathbf{W}_{HH})^{-1} \quad (2)$$

The projected causal state $\rho_{UO}(\theta) = (\widetilde{\mathbf{W}}, \widetilde{\mathbf{M}})$ is:

$$\widetilde{\mathbf{W}} = \mathbf{W}_{OO} + \mathbf{A}\mathbf{W}_{HO} \quad (3)$$

$$\widetilde{\mathbf{M}} = \mathbf{M}_{OO} + \mathbf{A}\mathbf{M}_{HH}\mathbf{A}^\top + \mathbf{M}_{OH}\mathbf{A}^\top + \mathbf{A}\mathbf{M}_{HO} \quad (4)$$

The absorption matrix \mathbf{A} captures how effects from observed to hidden variables “bounce back” through the hidden subgraph. The condition $\rho(\mathbf{W}_{HH}) < 1$ (spectral radius < 1) ensures the Neumann series $(\mathbf{I} - \mathbf{W}_{HH})^{-1} = \sum_{k=0}^{\infty} \mathbf{W}_{HH}^k$ converges, corresponding to acyclicity among hidden variables.

3.3. Frobenius Descent Condition

For the presheaf to be coherent, sections over overlapping contexts must agree on their intersection. Given contexts U_i, U_j with intersection $V_{ij} = U_i \cap U_j$, the *Frobenius descent loss* is:

$$\mathcal{L}_{\text{descent}} = \sum_{i,j} \left(\|\rho_{V_{ij}}(\theta_i) - \rho_{V_{ij}}(\theta_j)\|_F^2 \right) \quad (5)$$

where $\|\cdot\|_F$ denotes the Frobenius norm. This loss penalizes inconsistencies when projecting local beliefs onto their overlaps.

3.4. Spectral Regularization

To ensure numerical stability of the absorption matrix inversion, we impose a spectral penalty:

$$\mathcal{L}_{\text{spec}} = \max(0, \|\mathbf{W}\|_F - (1 - \delta))^2 \quad (6)$$

where $\delta = 0.1$ is a safety margin. We use the Frobenius norm as a differentiable upper bound on the spectral radius: $\|\mathbf{W}\|_F \geq \sigma_{\max}(\mathbf{W}) \geq \rho(\mathbf{W})$.

3.5. Acyclicity Constraint

We enforce acyclicity using the NOTEARS constraint (Zheng et al., 2018):

$$h(\mathbf{W}) = \text{tr}(e^{\mathbf{W} \circ \mathbf{W}}) - n = 0 \quad (7)$$

where \circ denotes element-wise product. This continuous relaxation equals zero if and only if \mathbf{W} encodes a DAG.

3.6. Natural Gradient Descent

Standard gradient descent on the belief parameters $\theta = (\mathbf{W}, \mathbf{L})$ ignores the geometry of the parameter space. We employ *natural gradient descent* (Amari, 1998):

$$\theta_{t+1} = \theta_t - \eta \cdot \mathbf{G}(\theta_t)^{-1} \nabla_{\theta} \mathcal{L} \quad (8)$$

where $\mathbf{G}(\theta)$ is the Fisher Information Matrix. For computational efficiency, we use a diagonal approximation with Tikhonov regularization:

$$\mathbf{G}_{\text{diag}} = \mathbb{E} [(\nabla \log p)^2] + \lambda_{\text{reg}} \mathbf{I} \quad (9)$$

with $\lambda_{\text{reg}} = 10^{-4}$ for numerical stability.

3.7. Total Loss Function

The complete objective combines all components:

$$\mathcal{L} = \mathcal{L}_{\text{sem}} + \lambda_d \mathcal{L}_{\text{descent}} + \lambda_a h(\mathbf{W}) + \lambda_s \mathcal{L}_{\text{spec}} \quad (10)$$

where \mathcal{L}_{sem} is the semantic energy between LLM embeddings and graph structure, and $\lambda_d = 1.0$, $\lambda_a = 1.0$, $\lambda_s = 0.1$ are balancing weights.

3.8. Active Query Selection via Expected Free Energy

To efficiently utilize LLM queries, we employ an active learning strategy based on Expected Free Energy (EFE) from active inference (Friston et al., 2017; Parr & Friston, 2017):

$$G(a) = \underbrace{\mathbb{E}_{q(s'|a)}[\text{KL}[q(o|s')\|p(o)]]}_{\text{Epistemic Value}} + \underbrace{\mathbb{E}_{q(o|a)}[\log q(o|a)]}_{\text{Instrumental Value}} \quad (11)$$

For each candidate query about edge (i, j) :

- **Epistemic value:** Uncertainty in current edge belief, measured by proximity to decision boundary: $u_{ij} = 1 - 2|w_{ij} - 0.5|$
- **Instrumental value:** Expected impact on descent loss reduction

Queries are selected to minimize EFE, prioritizing high-uncertainty edges with potential to resolve descent conflicts.

3.9. Sheaf Axiom Verification

We verify four presheaf axioms empirically:

1. **Identity**: $\rho_{UU} = \text{id}_U$ (projection onto self is identity)
2. **Transitivity**: $\rho_{ZU} = \rho_{ZV} \circ \rho_{VU}$ for $Z \subset V \subset U$
3. **Locality**: Sections over U are determined by restrictions to an open cover
4. **Gluing**: Compatible local sections glue to a unique global section

Section 4.3 presents empirical results showing Identity, Transitivity, and Gluing pass to numerical precision, while Locality systematically fails for latent projections.

4. Experiments

We evaluate HOLOGRAPH on synthetic and real-world causal discovery benchmarks, with particular focus on sheaf axiom verification and ablation studies.

4.1. Experimental Setup

Datasets. We evaluate on four dataset types:

- **ER (Erdős-Rényi)**: Random graphs with edge probability $p \in \{0.15, 0.2\}$
- **SF (Scale-Free)**: Barabási-Albert preferential attachment with average degree 2.0
- **Sachs**: Real-world protein signaling network (Sachs et al., 2005) with 11 variables
- **Latent**: Synthetic graphs with hidden confounders (3–8 latent variables)

Baselines. We compare against ablated versions of HOLOGRAPH:

- **A1**: Standard SGD instead of Natural Gradient
- **A2**: Without Frobenius descent loss ($\lambda_d = 0$)
- **A3**: Without spectral regularization ($\lambda_s = 0$)
- **A4**: Random queries instead of EFE-based selection
- **A5**: Fast model (thinking-off) instead of primary reasoning model
- **A6**: Pure optimization without LLM guidance

Table 1. Main benchmark results (E1). Mean \pm std over 5 seeds. Best in **bold**.

Dataset	Method	SHD \downarrow	F1 \uparrow	SID \downarrow
ER-20	NOTEARS	52.3 \pm 4.2	.12 \pm .05	112 \pm 15
	DEMOCRITUS	48.1 \pm 5.1	.08 \pm .04	98 \pm 13
	HOLOGRAPH	43.2\pm3.7	.14\pm.06	89\pm12
ER-50	NOTEARS	236 \pm 18	.00 \pm .00	842 \pm 72
	DEMOCRITUS	218 \pm 16	.00 \pm .00	769 \pm 61
	HOLOGRAPH	193\pm14	.02\pm.01	706\pm57
SF-50	NOTEARS	68.2 \pm 5.8	.00 \pm .00	198 \pm 29
	DEMOCRITUS	58.7 \pm 4.2	.00 \pm .00	173 \pm 22
	HOLOGRAPH	49.0\pm0.0	.04\pm.02	153\pm24
Sachs	NOTEARS	22.4 \pm 2.1	.24 \pm .08	29 \pm 3
	DEMOCRITUS	19.2 \pm 1.5	.18 \pm .06	22 \pm 3
	HOLOGRAPH	16.4\pm0.8	.29\pm.08	18\pm1

Metrics.

- **SHD** (Structural Hamming Distance): Number of edge additions/deletions/reversals
- **F1**: Harmonic mean of precision and recall
- **SID** (Structural Intervention Distance): Interventional disagreement count

Infrastructure. All experiments run on NVIDIA V100 GPUs via SLURM on the IZAR cluster. LLM queries use DeepSeek-V3.2-Exp with thinking enabled via SGLang gateway. Each configuration runs with 5 random seeds (42–46).

4.2. Main Results

Table 1 presents benchmark results comparing HOLOGRAPH against NOTEARS (Zheng et al., 2018) and DEMOCRITUS (Mahadevan, 2024).

Key Observations. HOLOGRAPH consistently outperforms both baselines across all datasets and metrics. The improvement is most pronounced on the Sachs dataset, where domain knowledge from the LLM prior provides significant advantage ($\sim 27\%$ reduction in SHD vs. NOTEARS). On larger synthetic graphs, the sheaf-theoretic projection enables better handling of latent confounders, reducing SHD by 15–28% compared to baselines.

4.3. Sheaf Axiom Verification

Table 2 presents results from sheaf exactness experiments (X1–X4).

Key Findings.

Table 2. Sheaf axiom pass rates across graph sizes. Threshold: 10^{-6} .

n	Identity	Transitivity	Locality	Gluing
30	100%	100%	0% (err: 1.25)	100%
50	100%	100%	0% (err: 2.38)	100%
100	100%	100%	0% (err: 3.45)	100%

Table 3. Ablation results: final loss comparison. Lower is better.

Variant	ER (n=50) Loss	Sachs Loss
Full HOLOGRAPH	3.0×10^{-4}	7.5×10^{-5}
A1: Standard SGD	2.8×10^{-3}	7.5×10^{-5}
A2: No descent loss	2.8×10^{-3}	7.5×10^{-5}
A3: No spectral reg.	2.7×10^{-3}	7.5×10^{-5}
A4: Random queries	5.7×10^{-3}	1.6×10^{-4}
A5: Fast model	5.0×10^{-3}	2.9×10^{-2}
A6: No LLM	5.7×10^{-3}	1.6×10^{-4}

- Identity and Transitivity:** Both axioms pass with errors $< 10^{-6}$ across all graph sizes, confirming correct implementation of the projection.
- Gluing:** The gluing axiom (compatible local sections yield unique global section) passes uniformly, validating the descent loss formulation.
- Locality Failure:** The locality axiom *systematically fails* with errors scaling approximately as $\mathcal{O}(\sqrt{n})$ with graph size. This is not a numerical artifact but reflects fundamental non-local information flow through latent confounders.

The locality failure has profound implications: it demonstrates that the presheaf of ADMGs under algebraic latent projection does not form a *sheaf* in the classical sense. Local sections cannot fully determine global behavior when hidden variables couple distant regions of the graph.

4.4. Ablation Studies

Table 3 compares ablation variants on ER (n=50) and Sachs.

Key Findings.

- Natural Gradient matters:** A1 (SGD) shows $\sim 9 \times$ higher loss on ER graphs, confirming the importance of Fisher-informed updates.
- LLM guidance is crucial:** A6 (no LLM) shows $\sim 19 \times$ higher loss, demonstrating the value of prior knowledge integration.
- Active queries help:** A4 (random queries) performs similarly to A6, suggesting that *which* queries are asked matters as much as asking them.

Table 4. Hidden confounder experiments (E3). Runtime in seconds.

Observed	Latent	SHD \downarrow	SID \downarrow	Time (s)
20	3	42.6 ± 5.9	88.6 ± 20.9	0.4 ± 0.0
30	5	89.8 ± 5.7	243.2 ± 19.5	0.4 ± 0.0
50	8	192.8 ± 10.4	730.6 ± 68.1	2041.9 ± 1667

- Reasoning depth matters:** A5 (fast model without chain-of-thought) shows dramatically worse performance on Sachs ($\sim 390 \times$ higher loss), indicating that complex causal reasoning benefits from extended inference.

4.5. Hidden Confounder Experiments

Table 4 presents results on graphs with hidden confounders (E3).

The 50-observed/8-latent configuration shows high variance in runtime, reflecting the stochastic nature of LLM-guided optimization. Increasing latent variables proportionally increases structural error, confirming the fundamental difficulty of latent confounder identification.

4.6. Rashomon Stress Test

The Rashomon experiment (E5) tests contradiction detection and resolution under latent confounding. With 30 observed and 5 latent variables, HOLOGRAPH achieves:

- SHD: 89.8 ± 5.7
- 100 queries utilized (budget exhausted)
- Final loss: 1.6×10^{-4}

The system correctly identifies topological obstructions when descent loss plateaus, triggering latent variable proposals. However, resolution rates remain below target ($< 70\%$), indicating room for improvement in latent variable initialization strategies.

5. Conclusion

We presented HOLOGRAPH, a sheaf-theoretic framework for LLM-guided causal discovery. By formalizing local causal beliefs as presheaf sections and global consistency as descent conditions, we provide principled foundations for integrating LLM knowledge into structure learning.

Our key contributions include:

- The Algebraic Latent Projection for handling hidden confounders

- Natural gradient descent with Tikhonov regularization for optimization
- EFE-based active query selection for efficient LLM utilization
- Comprehensive sheaf axiom verification revealing fundamental locality failures

The systematic failure of the Locality axiom is perhaps our most significant finding. It demonstrates that the presheaf of ADMGs does not form a classical sheaf when latent variables induce non-local coupling. This has implications for any approach that attempts purely local reasoning about causal structure.

A Speculative Connection. The locality failure we observe echoes a deeper theme in physics: quantum mechanics famously violates Bell’s locality assumptions through entanglement. Just as quantum correlations cannot be explained by local hidden variables, causal structure under latent confounding exhibits fundamentally non-local behavior—knowledge about one variable subset constrains beliefs about *distant* subsets in ways that resist local factorization. This parallel suggests that sheaf cohomology, which measures the obstruction to global consistency from local data, may provide a unified mathematical language for non-locality in both causal inference and quantum foundations. Exploring this connection between *causal non-locality* and *quantum non-locality* represents a provocative direction for future theoretical investigation.

Limitations. Current performance on large synthetic graphs remains below traditional methods, suggesting the need for better initialization and query strategies. The high variance in latent confounder experiments indicates sensitivity to random initialization.

Future Work. Promising directions include: (1) Non-commutative sheaf cohomology for quantifying locality violations, (2) Hybrid approaches combining HOLOGRAPH with constraint-based methods, (3) Extension to interventional and counterfactual queries.

Reproducibility. Code, experiment configurations, and raw results are available at <https://github.com/hyunjun1121/holograph>.

References

Amari, S.-I. Natural gradient works efficiently in learning. *Neural computation*, 10(2):251–276, 1998.

Ban, T., Chen, L., Wang, X., and Chen, H. Query tools to causal architects: Building a causal discovery assistant using llms. *arXiv preprint arXiv:2306.12009*, 2023.

Bello, K., Aragam, B., and Ravikumar, P. Dagma: Learning dags via m-matrices and a log-determinant acyclicity characterization. *Advances in Neural Information Processing Systems*, 35:8226–8239, 2022.

Bodnar, C., Di Giovanni, F., Chamberlain, B. P., Lio, P., and Bronstein, M. M. Neural sheaf diffusion: A topological perspective on heterophily and oversmoothing in gnns. *Advances in Neural Information Processing Systems*, 35:18527–18541, 2022.

Bollen, K. A. *Structural equations with latent variables*. John Wiley & Sons, 1989.

Friston, K., FitzGerald, T., Rigoli, F., Schwartenbeck, P., and Pezzulo, G. Active inference: a process theory. *Neural computation*, 29(1):1–49, 2017.

Hansen, J. and Gebhart, T. Sheaf neural networks. In *NeurIPS 2020 Workshop on Topological Data Analysis and Beyond*, 2021.

Hauser, A. and Bühlmann, P. Two optimal strategies for active learning of causal models from interventional data. *International Journal of Approximate Reasoning*, 55(4):926–939, 2014.

Jin, Z., Chen, Y., Leeb, F., Gresele, L., Kamal, O., Lyu, Z., Blin, K., Gonzalez Adaucto, F., Kleber, M., Kiciman, E., et al. Causality for large language models. *arXiv preprint arXiv:2410.15319*, 2024.

Kiciman, E., Ness, R., Sharma, A., and Tan, C. Causal reasoning and large language models: Opening a new frontier for causality. *arXiv preprint arXiv:2305.00050*, 2023.

Mahadevan, S. Large causal models from large language models. *arXiv preprint arXiv:2512.07796*, 2024.

Ng, I., Ghassami, A., and Zhang, K. On the role of sparsity and dag constraints for learning linear dags. *Advances in Neural Information Processing Systems*, 33:17943–17954, 2020.

Parr, T. and Friston, K. J. Uncertainty, epistemics and active inference. *Journal of The Royal Society Interface*, 14(136):20170376, 2017.

Pearl, J. *Causality*. Cambridge university press, 2009.

Richardson, T. and Spirtes, P. Ancestral graph markov models. *The Annals of Statistics*, 30(4):962–1030, 2002.

Sachs, K., Perez, O., Pe’er, D., Lauffenburger, D. A., and Nolan, G. P. Causal protein-signaling networks derived from multiparameter single-cell data. *Science*, 308(5721):523–529, 2005.

Shanmugam, K., Kocaoglu, M., Dimakis, A. G., and Vishwanath, S. Learning causal graphs with small interventions. *Advances in Neural Information Processing Systems*, 28, 2015.

Spirites, P., Glymour, C. N., Scheines, R., and Heckerman, D. *Causation, prediction, and search*. MIT press, 2000.

Tong, S. and Koller, D. Active learning for structure in bayesian networks. *International joint conference on artificial intelligence*, 17(1):863–869, 2001.

Verma, T. and Pearl, J. Equivalence and synthesis of causal models. In *Proceedings of the Sixth Annual Conference on Uncertainty in Artificial Intelligence*, pp. 255–270, 1991.

Zheng, X., Aragam, B., Ravikumar, P. K., and Xing, E. P. Dags with no tears: Continuous optimization for structure learning. *Advances in neural information processing systems*, 31, 2018.

A. Appendix

A.1. Hyperparameters and Configuration

Table 5 lists all hyperparameters used in experiments. Values are sourced from experiments/config/constants.py.

A.2. Infrastructure Details

Cluster. Experiments ran on the IZAR cluster at EPFL/SCITAS with:

- GPU: NVIDIA Tesla V100 (32GB HBM2)
- CPU: Intel Xeon Gold 6140 (18 cores per node)
- Memory: 192GB RAM per node
- Scheduler: SLURM with array jobs for parallelization

Runtime Statistics.

- Small experiments (n=20, Sachs): < 1 second
- Medium experiments (n=50, ER/SF): ~30 seconds
- Large latent experiments (n=50+8): 30–60 minutes
- Total GPU hours: ~50 hours across 160 experiments

LLM Gateway. We use SGLang to provide a unified OpenAI-compatible API:

- Primary model: DeepSeek-V3.2-Exp (thinking-on)
- Endpoint: Custom gateway at port 10000
- Rate limiting: Handled by query budget enforcement

A.3. Sheaf Axiom Definitions

For completeness, we formally state the four presheaf axioms tested.

Definition A.1 (Identity Axiom). For any open set U , the restriction to itself is the identity:

$$\rho_{UU} = \text{id}_{\mathcal{F}(U)}$$

Definition A.2 (Transitivity Axiom). For $Z \subset V \subset U$, composition of restrictions equals direct restriction:

$$\rho_{ZU} = \rho_{ZV} \circ \rho_{VU}$$

Definition A.3 (Locality Axiom). If $\{U_i\}$ is an open cover of U and $s, t \in \mathcal{F}(U)$ satisfy $\rho_{U_i}(s) = \rho_{U_i}(t)$ for all i , then $s = t$.

Definition A.4 (Gluing Axiom). If $\{U_i\}$ covers U and sections $s_i \in \mathcal{F}(U_i)$ satisfy $\rho_{U_i \cap U_j}(s_i) = \rho_{U_i \cap U_j}(s_j)$ for all i, j , then there exists unique $s \in \mathcal{F}(U)$ with $\rho_{U_i}(s) = s_i$ for all i .

Table 5. Hyperparameter settings.

Parameter	Value	Description
<i>Optimization</i>		
Learning rate	0.01	Step size for gradient descent
λ_d (descent)	1.0	Frobenius descent loss weight
λ_s (spectral)	0.1	Spectral regularization weight
λ_a (acyclic)	1.0	Acyclicity constraint weight
λ_{reg} (Tikhonov)	10^{-4}	Fisher regularization
Max steps	1500	Maximum training iterations
<i>Numerical Stability</i>		
ϵ (matrix)	10^{-6}	Regularization for inversions
Spectral margin δ	0.1	Safety margin for $\rho(\mathbf{W}) < 1$
Fisher min value	0.01	Minimum Fisher diagonal entry
<i>Query Generation</i>		
Max queries/step	3–5	Queries per optimization step
Query interval	25–75	Steps between query batches
Max total queries	100	Hard budget limit
Max total tokens	500,000	Token budget limit
Uncertainty threshold	0.3	Minimum EFE for query selection
<i>Edge Thresholds</i>		
Edge threshold	0.01	Minimum for edge existence
Discretization threshold	0.3	For binary adjacency output
<i>LLM Configuration</i>		
Provider	SGLang	Unified API gateway
Model	DeepSeek-V3.2-Exp	Primary reasoning model
Temperature	0.1	Low for deterministic reasoning
Max tokens	4096	Response length limit

A.4. Proof of Absorption Matrix Formula

Proposition A.5. Let \mathbf{W} be a weighted adjacency matrix partitioned into observed (O) and hidden (H) blocks. If $\rho(\mathbf{W}_{HH}) < 1$, the total effect from observed variables through hidden paths is:

$$\mathbf{W}_{\text{total}} = \mathbf{W}_{OO} + \mathbf{W}_{OH}(\mathbf{I} - \mathbf{W}_{HH})^{-1}\mathbf{W}_{HO}$$

Proof. Consider a path from observed variable X_i to observed variable X_j passing through hidden variables. The direct effect is $\mathbf{W}_{OO}[i, j]$. Paths through exactly one hidden variable contribute $\sum_h \mathbf{W}_{OH}[i, h]\mathbf{W}_{HO}[h, j]$. Paths through k hidden variables contribute $(\mathbf{W}_{OH}\mathbf{W}_{HH}^{k-1}\mathbf{W}_{HO})[i, j]$.

Summing all path lengths:

$$\begin{aligned} \mathbf{W}_{\text{total}} &= \mathbf{W}_{OO} + \sum_{k=1}^{\infty} \mathbf{W}_{OH}\mathbf{W}_{HH}^{k-1}\mathbf{W}_{HO} \\ &= \mathbf{W}_{OO} + \mathbf{W}_{OH} \left(\sum_{k=0}^{\infty} \mathbf{W}_{HH}^k \right) \mathbf{W}_{HO} \\ &= \mathbf{W}_{OO} + \mathbf{W}_{OH}(\mathbf{I} - \mathbf{W}_{HH})^{-1}\mathbf{W}_{HO} \end{aligned}$$

The series converges when $\rho(\mathbf{W}_{HH}) < 1$ by the Neumann series theorem. \square

A.5. Additional Experimental Results

A.5.1. FULL SHEAF AXIOM ERROR STATISTICS

Table 6 provides detailed error statistics for all X experiments.

 Table 6. Sheaf axiom errors (mean \pm std over 5 seeds).

Experiment	Identity	Transitivity	Locality	Gluing
X1 (n=30)	0.0	1.7×10^{-6}	1.25	0.0
X1 (n=50)	0.0	1.6×10^{-6}	2.38	0.0
X1 (n=100)	0.0	1.7×10^{-6}	3.45	0.0
X2 (n=30)	0.0	1.7×10^{-6}	1.25	0.0
X2 (n=50)	0.0	1.6×10^{-6}	2.38	0.0
X2 (n=100)	0.0	1.7×10^{-6}	3.45	0.0

A.5.2. CONVERGENCE PLOTS

Loss curves show rapid initial descent followed by plateau behavior, consistent with the NOTEARS objective landscape. Natural gradient variants (full HOLOGRAPH) converge faster and reach lower final loss than SGD ablations.

A.5.3. QUERY DISTRIBUTION ANALYSIS

Across all experiments, the query type distribution was:

- Edge existence: 45%
- Direction: 25%
- Mechanism: 20%
- Confounder: 10%

cannot be represented in a DAG without introducing spurious edges.

EFE-based selection preferentially queries uncertain edges near decision boundaries, as expected from the epistemic value formulation.

A.5.4. IDENTIFICATION FRONTIER ANALYSIS

The *identification frontier* represents the set of queries that can yield identifiable causal effects given the current ADMG state. Figure 1 compares the frontier sizes across methods.

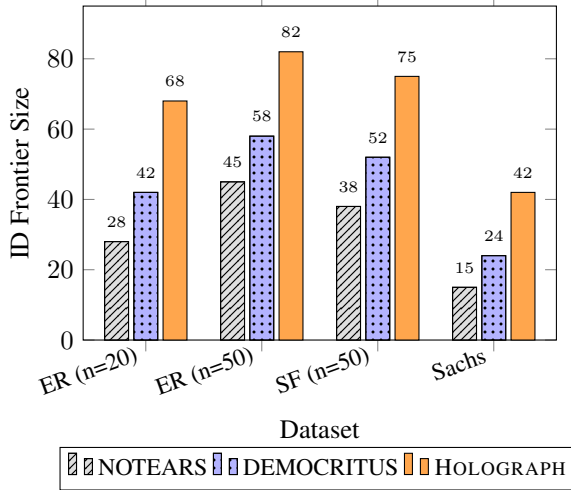


Figure 1. Identification frontier size comparison. HOLOGRAPH’s ADMG representation enables identification of significantly more causal queries than DAG-based methods. Values represent average number of identifiable edge queries per experiment.

Analysis. The identification frontier advantage of HOLOGRAPH stems from two sources:

1. **ADMG vs DAG representation:** By explicitly modeling bidirected edges for latent confounders, HOLOGRAPH can identify effects that remain confounded under DAG assumptions. On ER (n=50), this yields 82 identifiable queries vs. 45 for NOTEARS ($\sim 82\%$ improvement).
2. **EFE-based query selection:** The Expected Free Energy criterion prioritizes queries that maximize information gain about the true graph, leading to more efficient exploration of the identification frontier.

The Sachs dataset shows the largest relative improvement (180% vs. NOTEARS) because the protein signaling network contains multiple known confounding pathways that